POLYPUBLIE

Polarization-sensitive GeSn mid-infrared membrane photodetectors with integrated plasmonic metasurface

Ziqiang Cai, Cédric Lemieux-Leduc, Mahmoud R. M. Atalla, Lu Luo, Gérard Tanguy Eric Gnato Daligou, Simone Assali, Oussama Moutanabbir

Document en libre accès dans PolyPublie
Open Access document in PolyPublie

Date	2026
Type	Article de revue / Article
Version	Version officielle de l'éditeur / Published version
URL de PolyPublie PolyPublie URL	https://publications.polymtl.ca/74065/
Évaluation par les pairs Peer reviewed	Révisé par les pairs / Refereed
Conditions d'utilisation Terms of use	Creative Commons Attribution 4.0 International (CC BY)
Référence Citation	Cai, Z., Lemieux-Leduc, C., Atalla, M. R. M., Luo, L., Daligou, G. T. E. G., Assali, S., & Moutanabbir, O. (2026). Polarization-sensitive GeSn mid-infrared membrane photodetectors with integrated plasmonic metasurface. APL Photonics, 11(3), 036109 (9 pages). https://doi.org/10.1063/5.0313235

Publication officielle
Official publication

Titre de la revue Journal title	APL Photonics (vol. 11, no. 3)
Maison d'édition Publisher	AIP Publishing
URL officielle Official URL	https://doi.org/10.1063/5.0313235
Mention légale Legal notice	© 2026 Author(s). All article content, except where otherwise noted, is licensed under a Creative Commons Attribution (CC BY) license (https://creativecommons.org/licenses/by/4.0/).

Ce fichier a été téléchargé à partir de PolyPublie, le dépôt institutionnel de Polytechnique Montréal
This file has been downloaded from PolyPublie, the institutional repository of Polytechnique Montréal
https://publications.polymtl.ca

APL Photonics

RESEARCH ARTICLE | MARCH 23 2026

Polarization-sensitive GeSn mid-infrared membrane photodetectors with integrated plasmonic metasurface

Ziqiang Cai ; Cédric Lemieux-Leduc ; Mahmoud R. M. Atalla ; Lu Luo ; Gérard Daligou ; Simone Assali ; Oussama Moutanabbir

Check for updates

APL Photonics 11, 036109 (2026)
https://doi.org/10.1063/5.0313235

View Online
Export Citation

Articles You May Be Interested In

Extended short-wave infrared high-speed all-GeSn PIN photodetectors on silicon

APL Photonics (May 2024)

Recrystallization and interdiffusion processes in laser-annealed strain-relaxed metastable $Ge_{0.89}Sn_{0.11}$

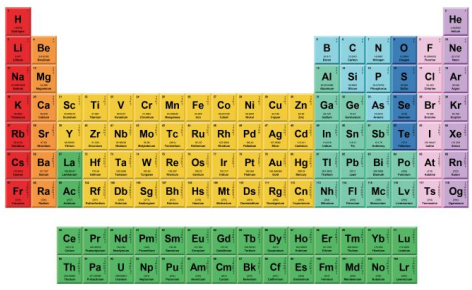
J. Appl. Phys. (March 2022)

Pseudo single crystal, direct-band-gap $Ge_{0.89}Sn_{0.11}$ on amorphous dielectric layers towards monolithic 3D photonic integration

Appl. Phys. Lett. (November 2014)

03 November 2026 17:51:32

AMERICAN ELEMENTS
THE MATERIALS SCIENCE MANUFACTURER®
Now Invent.™
29th ANNIVERSARY 1997 – 2026



American Elements
Opens a World of Possibilities
...Now Invent!
www.americanelements.com
© 1997-2026. American Elements is a U.S. Registered Trademark

AIP Publishing

Polarization-sensitive GeSn mid-infrared membrane photodetectors with integrated plasmonic metasurface

Cite as: APL Photon. 11, 036109 (2026); doi: 10.1063/5.0313235
Submitted: 21 November 2025 • Accepted: 4 March 2026 •
Published Online: 23 March 2026

View Online Export Citation CrossMark

Ziqiang Cai, Cédric Lemieux-Leduc, Mahmoud R. M. Atalla, Lu Luo, Gérard Daligou, Simone Assali, and Oussama Moutanabbir[a)]

AFFILIATIONS

Department of Engineering Physics, École Polytechnique de Montréal, Montréal, C.P. 6079, Succ. Centre-Ville, Montréal, Québec H3C 3A7, Canada

[a)]Author to whom correspondence should be addressed: oussama.moutanabbir@polymtl.ca

ABSTRACT

Germanium–tin (GeSn) semiconductors are promising for mid-infrared photodetectors owing to their silicon compatibility, tunable bandgap, and potential for room-temperature operation. Released GeSn membranes provide an additional degree of freedom to extend the operation wavelength through epitaxial strain relaxation, while their transferability expands design flexibility. Meanwhile, metasurfaces have become an effective strategy for engineering light–matter interactions, and their integration with photodetectors can enhance performance and introduce new functionalities. Here, we demonstrate a mid-infrared photodetector consisting of a transfer-printed $Ge_{0.89}Sn_{0.11}$ membrane integrated with a Au plasmonic metasurface. The photodetector exhibits a wavelength cutoff exceeding 3.0 μm and a nearly fourfold increase in responsivity at 2.5 μm compared to unreleased films, attributed to Fabry–Pérot resonance. Furthermore, by introducing an anisotropic metasurface, the obtained detectors display a strong polarization sensitivity, achieving a measured contrast ratio of ~4:1 between orthogonal polarizations. Moreover, the operation wavelength of the photodetector can be selectively tuned by varying the geometric scale of the metasurface. The experimental results show excellent agreement with simulations, confirming the effectiveness and versatility of this integrated metasurface-membrane design.

© 2026 Author(s). All article content, except where otherwise noted, is licensed under a Creative Commons Attribution (CC BY) license (https://creativecommons.org/licenses/by/4.0/). https://doi.org/10.1063/5.0313235

03 November 2026 17:51:32

INTRODUCTION

Mid-infrared (MIR) photodetectors hold strategic importance for sensing and imaging applications, yet their development is hindered by a limited selection of suitable materials.[1] Among the emerging candidates, GeSn alloys have attracted considerable attention as a group-IV platform with tunable optical properties extending into the MIR.[2] Over the past decade, GeSn-based devices have been studied in a variety of room-temperature MIR photodetectors operating between wavelengths of 1.6 and 4 μm,[3] including p–i–n photodetectors,[4] multiple-quantum-well (MQW) photodetectors,[5] waveguide photodetectors,[6] and nanoscale photodetectors.[7,8] In addition, GeSn alloys have been investigated for other MIR optoelectronic components, such as LEDs,[9,10] lasers,[11,12] and modulators.[13] These alloys can be grown epitaxially on Ge/Si substrates, providing compatibility with silicon processing standards.[2] Increasing the Sn composition narrows the bandgap energy of the GeSn alloy. Notably, an indirect-to-direct bandgap transition occurs above 7 at. % Sn in a fully relaxed alloy,[2] significantly improving light absorption and emission. Further Sn incorporation extends the cutoff wavelength deeper into the MIR range.[14] Furthermore, the cutoff wavelength of GeSn can also be tuned via engineering its internal strain, by means of controlling the GeSn thickness[15] or etching the underlying sacrificial layer.[16] When the Ge buffer layer is completely removed, the top GeSn layer can be released as a membrane, which relaxes the residual compressive strain and further extends the cutoff wavelength.[14] Moreover, GeSn membranes offer additional advantages, including reduced dark current and photocarrier recombination due to interfacial defect removal,[14] enhanced responsivity,[17] and integration on flexible substrates[18] relevant for printed electronics.[19] The GeSn

membranes can also be implemented in mainstream microelectronics. In our previous studies, we have successfully fabricated an array of GeSn membrane photodetectors[20] and integrated the membranes with Si waveguides to make on-chip photodetectors.[21] In addition, rolling-based large-area transfer of semiconductor membranes has been demonstrated.[22] While membranes made of semiconductors such as Si or Ge have been extensively studied[23] and even mass-produced for commercial photonic applications,[22] research on GeSn membranes is still in its early stage.

Meanwhile, metasurfaces have emerged as powerful tools for advancing photodetector engineering. As planar, subwavelength arrays of meta-atoms, metasurfaces provide unprecedented control over light by locally manipulating its amplitude, phase, and polarization through careful design of the geometry of each meta-atom, exhibiting enhanced performance and unique functionalities.[24] This capability has spurred significant research efforts to harness metasurfaces for enhancing key detector performance metrics, including spectral bandwidth, responsivity, and operational speed.[25–27] Metasurfaces have been applied in different kinds of photodetectors, such as two-dimensional (2D) material photodetectors,[28] quantum-dot photodetectors,[29] hot-electron photodetectors,[30] pyroelectric photodetectors,[31] terahertz photodetectors,[32] and avalanche photodetectors.[33] Ge and GeSn photodetectors integrated with metasurfaces have also been the subject of recent studies.[34–39] Beyond performance boosting, metasurfaces can also incorporate new functionalities, enabling polarization and multi-dimensional and spectral detections.[25] A photodetector integrated with an asymmetric nanobar array, for example, gains polarization-sensitive responsivity, while combining multiple oriented metasurfaces allows for the measurement of full Stokes parameters.[40–42] This polarization-dependent responsivity forms the basis of a MIR polarization sensor, enabling applications in material texture analysis and label-free biomedical diagnostics by probing microstructures through their intrinsic birefringence and polarization-dependent scattering properties. This capability opens the path toward compact, on-chip sensors suitable for real-time analysis and point-of-care diagnostics.[43] Despite this rapid progress in metasurface-integrated photodetectors, the specific combination of a metasurface with a transfer-printed GeSn membrane remains underexplored despite its importance for MIR sensing applications. It is noteworthy that the release of the GeSn membrane is beneficial at three distinct levels: (1) strain relaxation and the associated extension of the operational wavelength toward longer MIR wavelengths; (2) removal of the underlying defective layer originating from lattice-mismatched growth, thereby reducing carrier trapping and nonradiative recombination; and (3) enhanced flexibility in device design and fabrication, enabling architectures that are difficult to realize on rigid substrates or using as-grown materials.

In this work, we demonstrate a novel MIR photodetector that integrates transfer-printed GeSn membranes with anisotropic Au plasmonic metasurfaces. The device was fabricated by first epitaxially growing a GeSn layer (11 at. % Sn) on a Si wafer with Ge as an interlayer. The $Ge_{0.89}Sn_{0.11}$ layer was then patterned and released as a membrane via selective etching of the buffer layer and transfer-printed onto a SiO_2/Si substrate.[20] The high refractive index contrast between the GeSn membrane and the SiO_2 substrate enhances Fabry–Pérot (FP) resonances, yielding a nearly fourfold increase in responsivity at the FP resonance (2.5 μm) compared to unreleased films. Moreover, the subsequent integration of an Au metasurface makes the photodetector polarization-selective. The responsivity contrast ratio measured at 2.2 μm is ~4:1 between orthogonal polarizations. Numerical simulations corroborate the experimental results, showing excellent agreement and validating the proposed design. Finally, we demonstrate that the operating wavelength of the photodetector can be selectively tuned by varying the geometric scale of the metasurface. This result underscores the design flexibility enabled by the integration of free-standing membranes with metasurfaces, providing a versatile platform for wavelength-specific photodetection in the MIR.

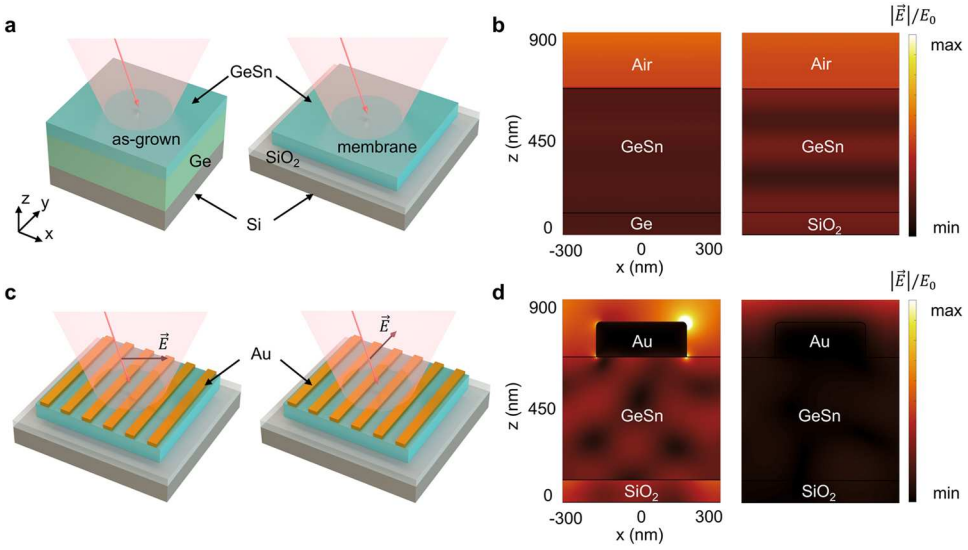


FIG. 1. Designs of the GeSn membrane photodetectors. (a) Schematics of the as-grown GeSn photodetector (left) and the transferred membrane photodetector (right). (b) Corresponding electric field amplitude distributions of the as-grown (left) and membrane (right) photodetectors. (c) Schematics of the membrane photodetector integrated with an Au metasurface, with an incident electric field to be TM-polarized (left) and TE-polarized (right). (d) Corresponding electric field amplitude distributions for TM-polarized (left) and TE-polarized (right) electric fields, respectively. For (b) and (d), the wave vector of incident light is inside the xz-plane with an incident angle of 30°, and the wavelength is 2.2 μm. $|\vec{E}|/E_0$ refers to the electric field amplitude divided by an incident electric field amplitude.

03 November 2026 17:51:32

© Author(s) 2026

RESULTS AND DISCUSSION

Conventionally, devices are fabricated by epitaxially growing a Ge buffer layer followed by a GeSn layer on a silicon substrate to mitigate defects arising from lattice mismatch [Fig. 1(a), left panel]. The performance of the device can be enhanced by releasing the GeSn membrane through etching the Ge buffer layer and transferring it onto a SiO_2/Si substrate [Fig. 1(a), right panel]. This structure serves multiple purposes. First, the released strain extends the photodetector's cutoff wavelength from ~2.8 to 3.2 μm, as discussed below. Second, the etching of the underlying layers to release the membranes removes the defective region, which consequently minimizes defect-related traps, thus lowering the recombination rate of photogenerated carriers. Third, the high refractive index contrast between GeSn (n = 4.28) and SiO_2 (n = 1.44) enables a strong FP resonance within the GeSn layer, thereby enhancing light absorption. Finally, the SiO_2 layer acts as an electrically insulating layer for subsequent measurements. To elucidate the influence of the GeSn membrane structure on photodetector performance, we simulated their electric field distributions [Fig. 1(b)]. Since a Cassegrain lens was used to focus light onto the sample, an oblique incidence angle was adopted in the simulation to match the experimental configuration. More details on the simulation can be found in the Methods section, and the refractive index of GeSn can be found in Sec. 1 of the supplementary material. As illustrated in Fig. 1(b), the distinct fringes in the electric field amplitude distribution within the GeSn membrane confirm excitation of this FP resonance. However, in the as-grown device, the resonance is significantly weaker. This FP resonance can be further enhanced by adding a highly reflective layer on the Si substrate, such as an Au layer,[44] as will be demonstrated in Fig. 4(e), or a distributed Bragg reflector (DBR).[17] In addition, the FP resonance can also be enhanced by increasing the thickness of the SiO_2 layer, or directly using a silica substrate, which can reduce the leakage of light into the substrate.[45]

The integration of a metallic metasurface on top of the GeSn membrane photodetector introduces polarization sensitivity into the device. As shown in Fig. 1(c), a one-dimensional periodic Au grating (150 nm thick, 380 nm width, 710 nm period, optimized to have the highest responsivity at 2.2 μm) was applied to the membrane. This anisotropic structure produces distinct optical responses for orthogonal light polarizations. Figure 1(d) illustrates the underlying mechanism: under transverse-magnetic (TM) polarized plane wave illumination (electric field polarized in the xz-plane), a strong localized enhancement of the electric field occurs due to the excitation of plasmonic resonance [Fig. 1(d), left panel]. In contrast, transverse-electric (TE) polarized light (electric field polarized along the y-axis) fails to excite this resonance, resulting in a markedly weaker field intensity [Fig. 1(d), right panel], making our device polarization-dependent. Moreover, the geometry of the metasurface also determines the optical resonance characteristics. By adjusting structural parameters such as period and width, resonant wavelengths can be precisely tailored. A detailed analysis of this spectral tuning behavior is presented in Fig. 4.

The device was fabricated according to the process flow illustrated in Fig. 2(a): (i) sequential deposition of a 1.02 μm Ge buffer layer and a 520 nm $Ge_{0.89}Sn_{0.11}$ layer on a Si substrate via chemical vapor deposition (CVD); (ii) patterning of 20 × 20 μm^2 mesas via photolithography and wet etching, followed by a dry etching step using CF_4 gas to selectively undercut the Ge buffer layer; (iii) detach of the GeSn membranes from the original substrate using a PDMS stamp; (iv) transfer printing of the membranes onto a

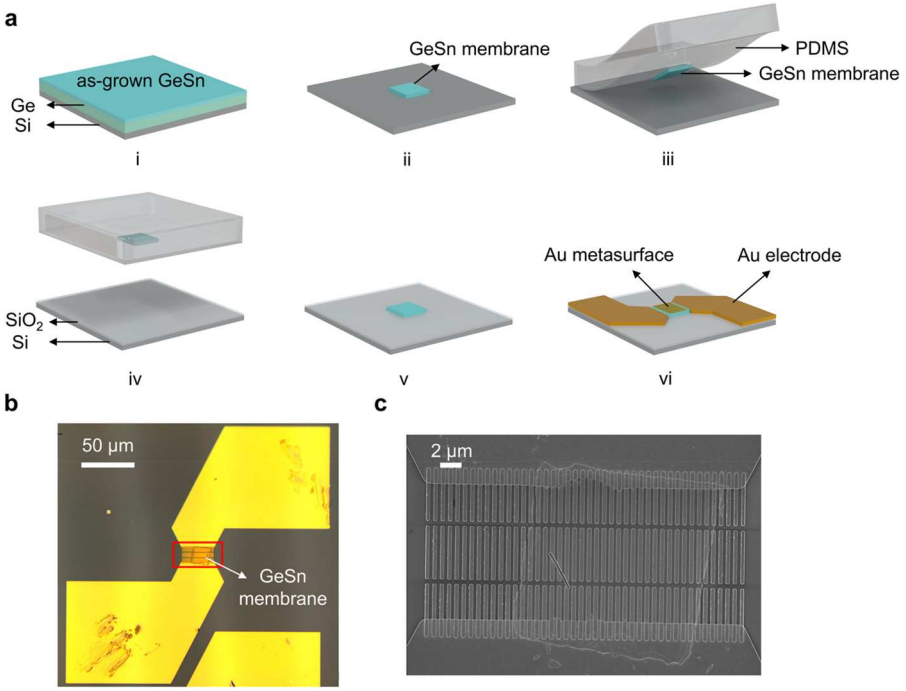


FIG. 2. (a) Fabrication steps of the GeSn membrane photodetector integrated with an Au metasurface. (b) Optical image of the fabricated device. The red box marks the area of the SEM image. (c) SEM image of the metasurface on top of the GeSn membrane.

03 November 2026 17:51:32

© Author(s) 2026

SiO_2/Si substrate; (v) post-transfer cleaning and annealing of the membranes; and (vi) fabrication of Au electrodes and the metasurface via a combination of photolithography and electron-beam lithography (EBL). More details on the GeSn growth and fabrication process can be found in the Methods section.

An optical micrograph of the final device is shown in Fig. 2(b), where the GeSn membrane is contacted by electrodes at both ends and the metasurface is positioned on top. For optoelectrical characterization, a small bias voltage was applied across the electrodes via micromanipulator probes, and the resulting current was measured. The incident light generates photocarriers within the membrane, leading to a measurable photocurrent (I_{photo}) corresponding to the increase in current above the baseline dark current (I_{dark}). The electrical signals were sent to either a Fourier transform spectrometer (FTIR) to retrieve the relative responsivity spectrum, or a source measure unit to measure the absolute responsivity. More details on the FTIR and absolute responsivity measurements can be found in Sec. 2 of the supplementary material. Figure 2(c) shows a scanning electron microscopy (SEM) image of the metasurface region, confirming the fabrication quality of the metasurface and its precise alignment over the GeSn membrane.

The performance of the GeSn photodetectors was investigated through both numerical simulations and experimental studies. In the simulations [Figs. 3(b) and 3(e)], the responsivity was estimated

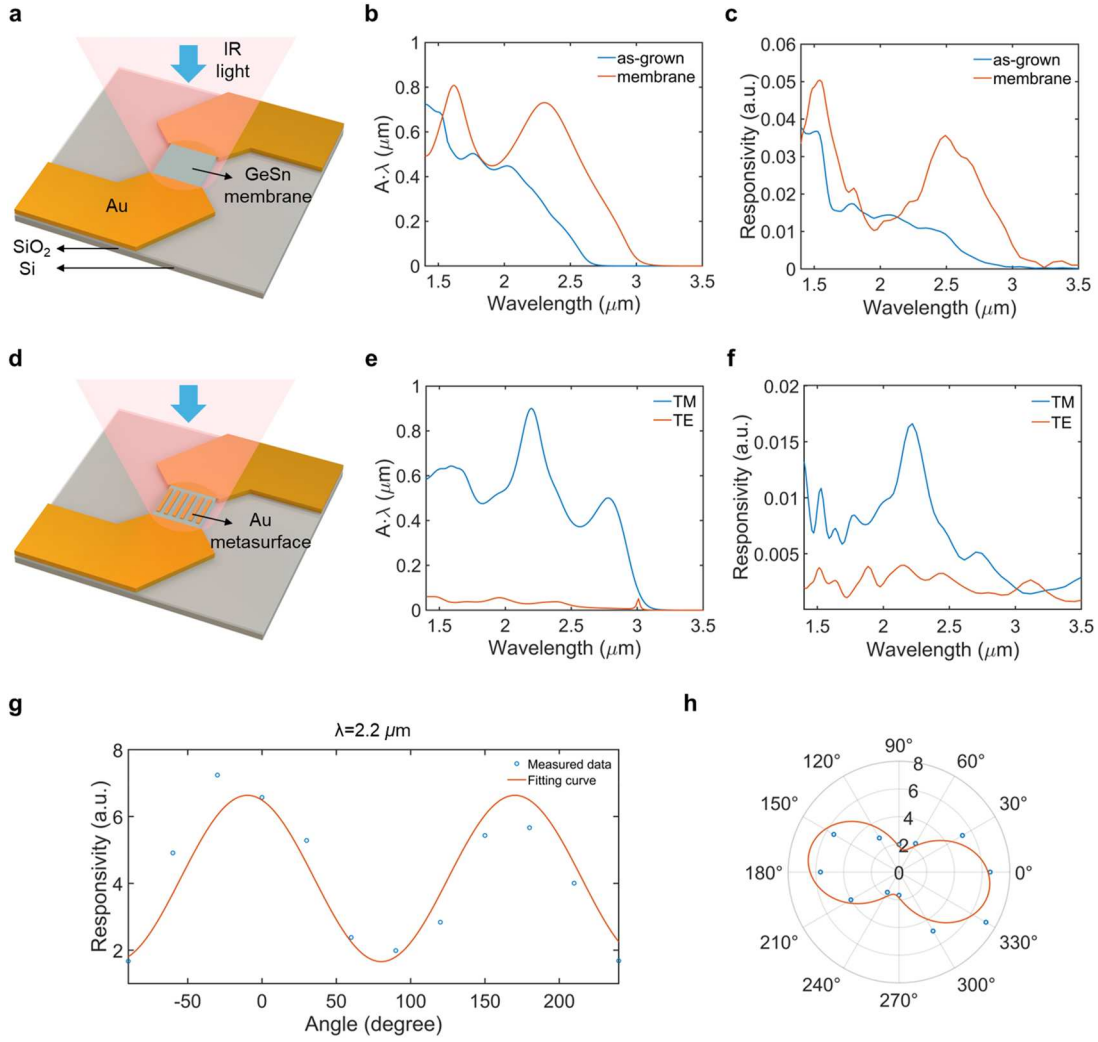


FIG. 3. Simulated and measured responsivity spectra of the GeSn photodetectors. (a) Schematic of the GeSn membrane photodetector without a metasurface. (b) Simulated responsivity spectra for the as-grown GeSn photodetector (blue curve) and the GeSn membrane photodetector (red curve). (c) Relative responsivity spectra for the as-grown photodetector (blue curve) and the membrane photodetector (red curve) measured by FTIR (a.u. stands for arbitrary units). (d) Schematic of the GeSn membrane photodetector integrated with a metasurface. (e) Simulated responsivity spectra for TM-polarized (blue curve) and TE-polarized (red curve) incident light. (f) Relative responsivity spectra for TM-polarized (blue curve) and TE-polarized (red curve) incident light measured by FTIR. (g) Measured responsivity at 2.2 μm vs polarizer angle (blue dots), together with a fitting curve (red line). (h) Corresponding polar diagram.

03 November 2026 17:51:32

© Author(s) 2026

from the product of light absorption (A) in GeSn and Ge and wavelength (λ), based on the principle that responsivity is proportional to the absorbed light intensity divided by the photon energy. Figure 3(b) illustrates a key distinction between the as-grown and membrane-based devices. For the as-grown photodetector, both the GeSn layer and the underlying Ge buffer contribute to the photoresponse. This results in a characteristic step in the responsivity curve near 1.6 μm, where the Ge contribution begins to decline, diminishing entirely at its cutoff wavelength of 1.8 μm. The GeSn absorption itself falls to zero near its cutoff wavelength of 2.7 μm. In contrast, the GeSn membrane photodetector exhibits a responsivity spectrum with FP resonances. As previously discussed in Fig. 1(b), these resonances enhance the local optical field within the membrane, thereby boosting the responsivity at resonant wavelengths. Furthermore, strain relaxation associated with the membrane release extends the GeSn cutoff wavelength from 2.7 to 3.1 μm. The combined effect of resonant enhancement and a broader spectral range results in a significantly higher responsivity across the 2–3 μm wavelength range. The experimental data, presented in Fig. 3(c), show excellent agreement with the simulated results. The measured cutoff wavelength extends from ~2.8 to 3.2 μm after membrane releasing, and the responsivity exhibits an enhancement of nearly fourfold at 2.5 μm. A minor discrepancy is observed in the membrane device, where the measured resonant peak at longer wavelengths is slightly redshifted compared to the simulation. This small shift is likely due to the discrepancy between the GeSn refractive index used in the model, which was derived from eight-band $k \cdot p$ method calculations, and the real refractive index of GeSn. More details on the refractive index used in simulations are provided in Sec. 1 of the supplementary material.

To incorporate polarization sensitivity into the device, an Au metasurface was fabricated on the GeSn membrane. The simulated results in Fig. 3(e) reveal a sharp resonant peak at 2.2 μm for TM-polarized light, while the responsivity to TE-polarized light is negligible. This high contrast originates from the polarization-selective nature of the anisotropic structure. The TM-polarized light can efficiently excite plasmonic resonance, leading to strong local field enhancement, whereas the TE-polarized light is effectively blocked by the metallic grating. The experimental results in Fig. 3(f) show a resonant peak for TM-polarization and a flat, low response for TE-polarization, agreeing with simulation results. However, the measured polarization contrast is lower than the simulated. We attribute this discrepancy to the finite size of the fabricated membrane, considering that our simulations employed periodic boundary conditions that model an infinite array. To validate this explanation, a systematic study showing how the membrane dimensions affect the simulated response is provided in Sec. 3 of the supplementary material. To further investigate the photodetector's polarization sensitivity, we gradually rotate the polarizer and measure the responsivity spectrum at each angle. The corresponding results are presented in Figs. 3(g) and 3(h). The data were fitted with the function $R_x \times \cos^2(\theta_{pol} + \theta_0) + R_y \times \sin^2(\theta_{pol} + \theta_0)$, where R_x and R_y represent the responsivities for light polarized along the x- and y-axes, respectively, θ_{pol} is the polarization angle, and θ_0 is the offset angle. By fitting the data, we retrieve the contrast ratio, defined as R_x/R_y, to be 4.0. The original FTIR spectra measured at different angles of polarizer can be found in Sec. 4 of the supplementary material.

The results shown in Figs. 3(c) and 3(f) are extracted directly from the FTIR spectrometer and thus are not absolute responsivity values. To quantify the absolute values, we supplemented the relative spectral data from FTIR measurements with absolute responsivities measured at 1.55 μm. This allowed us to deduce the absolute responsivities at the wavelength of interest. At the bias voltage V_b of 30 mV and a wavelength λ of 2.2 μm, the deduced responsivities for the as-grown and metasurface-integrated membrane photodetectors are 1.52 and 2.01 mA/W, respectively (details can be found in Sec. 5 of the supplementary material). The metasurface-integrated device thus shows an enhancement factor of ~1.3 compared to the as-grown GeSn photodetector. This value is lower than the enhancement that the GeSn membrane photodetector without a metasurface exhibits at 2.5 μm. The greater enhancement of nearly fourfold at 2.5 μm is attributed to its proximity to the cutoff wavelength of the as-grown GeSn detector, where the responsivity drops. Furthermore, we anticipate that the measured responsivity of the metasurface-integrated device can be further enhanced by optimizing the fabrication process to minimize defects, such as membrane edge roughness and metasurface imperfections.

The metasurface not only provides polarization selectivity but also enables spectral tunability. The hybrid structure combining the metasurface with the underlying membrane forms an asymmetric FP resonator,[46] in which the metasurface acts as the front mirror and the GeSn/SiO_2 interface serves as the back mirror. The plasmonic resonance of the metasurface imparts an abrupt phase shift to incident light, and modifying the geometry of the metasurface allows this phase shift to be adjusted. This in turn modifies the interference condition within the cavity, thereby tuning the resonant wavelength. To explore the tunability of the metasurface, we simulated the photodetector's responsivity spectra across a range of parameters. As shown in Fig. 4(a), the width and period of the nanoribbons are scaled by the same scale factor (scale), while all other parameters remain constant. In Fig. 4(b), as the scale increases from 0.8 to 1.0, the resonant peak at shorter wavelength redshifts from 2.0 to 2.2 μm, and another resonant peak at longer wavelength redshifts from 2.4 to 2.8 μm. The resonant wavelength can also be tuned by varying the GeSn layer thickness (t_{GeSn}). As shown in Figs. 4(c) and 4(d), increasing t_{GeSn} from 450 to 550 nm shifts the resonance from 2.1 to 2.3 μm. These results confirm that the resonant wavelength can be tuned through either metasurface dimensions or GeSn thickness with a high degree of control. However, for practical device fabrication, tuning the metasurface dimensions offers a superior advantage compared to modifying the GeSn thickness, since the metasurfaces with different dimensions can be easily fabricated on the same substrate, while thicker GeSn layers are difficult to grow given their metastable nature and large lattice mismatch compared to Ge/Si growth wafers. Furthermore, in our previous work, we have demonstrated the transfer printing of an array of GeSn membranes onto a substrate of choice.[20,21] By fabricating a distinct metasurface on each membrane, where each metasurface is engineered with a specific geometric scale to resonate at the target wavelength or with a defined orientation to resolve individual Stokes parameters, it is possible to develop a MIR photodetector for multiwavelength and full-Stokes detection.[41,42] Moreover, the responsivity can be further enhanced by introducing an additional highly reflective Au layer between the SiO_2 and Si layers. As illustrated in Fig. 4(e), the top metasurface, together with the GeSn membrane and SiO_2 layer atop

03 November 2026 17:51:32

© Author(s) 2026

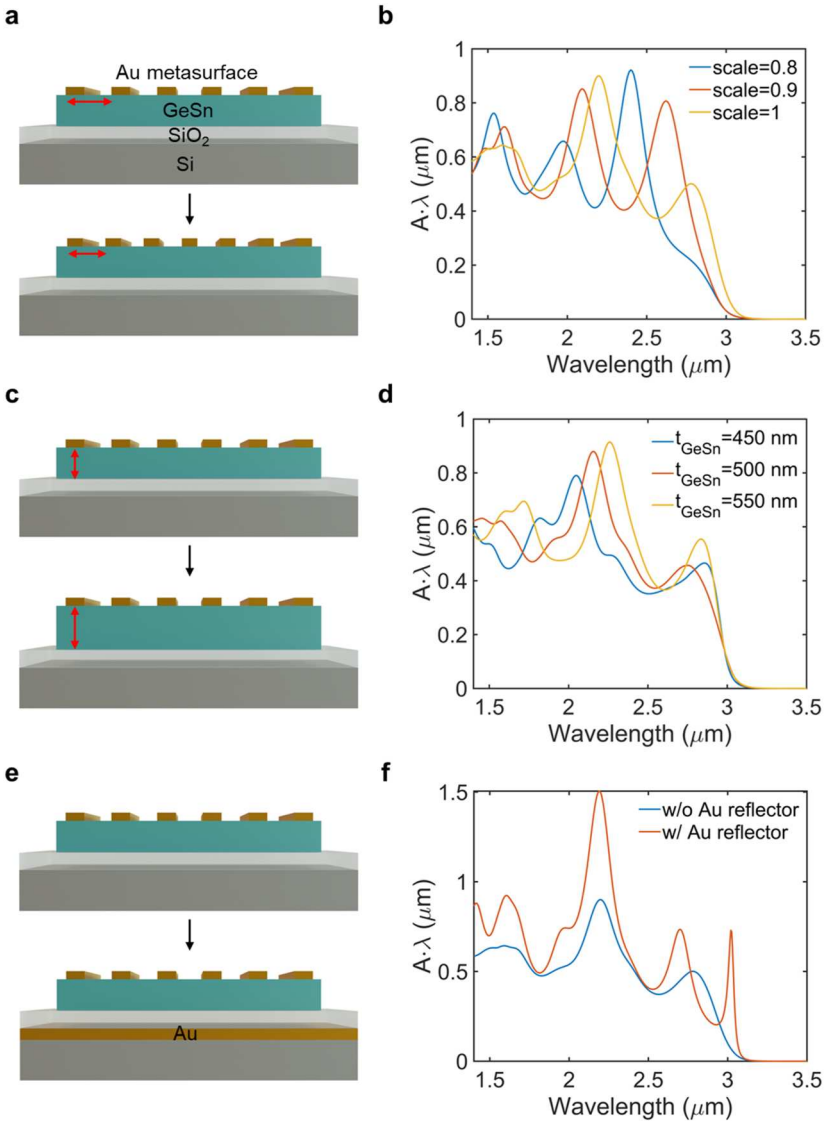


FIG. 4. [(a) and (b)] Geometry and performance of the metasurface-tuned photodetectors. (a) Schematics with varying metasurface scales. (b) Corresponding simulation results of the responsivity spectra, showing tuning of resonant wavelengths. [(c) and (d)] Geometry and performance of the thickness-tuned photodetectors. (c) Schematics with varying GeSn layer thicknesses. (d) Corresponding simulation results. The red arrows in [(a) and (c)] mark the changes in geometry. (e) Schematics without (top) and with (bottom) an Au reflector layer. (f) Corresponding simulation results.

the bottom Au layer, forms a metal–insulator–metal (MIM) structure. Under critical coupling conditions, this configuration enables perfect light absorption.[46] The resulting enhancement in optical absorption within the GeSn layer increases the responsivity by nearly 70% at 2.2 μm, as shown in Fig. 4(f). Finally, we simulated the responsivity spectra as a function of nanoribbon width while maintaining a constant period, with the results provided in Sec. 6 of the supplementary material. The simulations reveal that the peak responsivity initially increases and then decreases with an increasing Au grating filling ratio. This behavior confirms that the metasurface does not simply block incident light but couples light into plasmonic resonances, offering multiple degrees of freedom to tailor the photodetector's performance.

CONCLUSION

We have demonstrated a polarization-sensitive MIR photodetector by integrating an Au plasmonic metasurface onto the transfer-printed $Ge_{0.89}Sn_{0.11}$ membrane. Releasing the membrane by etching the underlying Ge layer redshifts the cutoff wavelength from 2.7 to 3.1 μm. When transferred to a low refractive index substrate, the integrated detector exhibits FP resonances that enhance responsivity in the 2–3 μm wavelength range, with nearly fourfold enhancement at 2.5 μm, compared to as-grown devices. The metasurface-integrated photodetector displays strong polarization sensitivity, with a measured contrast ratio of 4.0 at 2.2 μm. Furthermore, by modifying the metasurface geometry, the resonant wavelength can be tuned within the 2.0–2.8 μm range. This approach

03 November 2026 17:51:32

© Author(s) 2026

can broaden the application of GeSn photodetectors, paving the way for high performance room temperature multifunctional MIR photodetectors.

METHODS

Numerical simulation

We performed numerical simulations using the Electromagnetic Waves, Frequency Domain module in COMSOL Multiphysics. A 2D model with Floquet periodic boundary conditions, in which in-plane wave vectors were taken from the periodic port, was employed to simplify the calculations. Linearly polarized plane waves with either TM or TE polarizations were applied as incident lights. The angle of incidence is 30° to match the Cassegrain lens configuration of our experimental setup, considering that the numerical aperture (NA) of the lens is 0.5. A detailed discussion on how the Cassegrain lens configuration was considered in simulation can be found in Sec. 7 of the supplementary material. Absorptions of light in GeSn and Ge were calculated by integrating the electromagnetic power loss density over the GeSn and Ge areas and then dividing by the input power.

Epitaxial growth of GeSn layers

The $Ge_{0.89}Sn_{0.11}$ alloy growth was carried out in a low-pressure chemical vapor deposition (LPCVD) reactor on a 4-in. Si (100) wafer. First, a 1.02 μm-thick Ge virtual substrate (Ge-VS) was grown using 10% monogermane (GeH_4) and a continuous flow of pure hydrogen following a two-temperature growth protocol at 460 and 600 °C. In addition to reducing the lattice mismatch between the Si substrate and GeSn, Ge-VS also acts as a sacrificial layer, facilitating the GeSn membranes under etching and release. Subsequently, the $Ge_{0.89}Sn_{0.11}$ layers were grown on Ge/Si wafers at 320 °C using GeH_4 and $SnCl_4$ precursors. The microstructure of the as-grown material was assessed using cross-sectional transmission electron microscopy, and the Sn composition was determined through x-ray diffraction with reciprocal space mapping.

Fabrication

The device was fabricated following the process flow in Fig. 2(a). For membrane fabrication, after the epitaxial growth of the GeSn layer, we first diced the wafer. Then, we spin-coated photoresist (PR) onto the chip and used photolithography to define the patterns of GeSn membranes, followed by a post-bake process to enhance the adhesion between the PR and the GeSn layer. Next, the patterned PR was used as an etch mask, and the unprotected areas were etched using a Cr etchant solution. After removing the PR with acetone, the remaining Ge layer was removed using reactive ion etching (RIE) with CF_4 gas. After GeSn membranes were fabricated, we used a PDMS stamp coated with polycarbonate to catch the membranes. Following that, the PDMS with the membranes was pressed onto a new substrate, which was prepared by depositing a 100 nm SiO_2 layer on a silicon wafer using plasma-enhanced chemical vapor deposition (PECVD). Then, the substrate was heated to 180 °C to melt the polycarbonate, and the PDMS stamp was lifted with membranes remaining on the substrate, followed by a cleaning process to remove the polycarbonate from the membranes. Afterward, we used another round of photolithography to pattern the electrodes. We deposit 5 nm Ti and 150 nm Au by e-beam evaporation and the lift-off process to fabricate the electrodes. Finally, we used the EBL process to define the metasurface patterns, followed by another round of e-beam evaporation to deposit 5 nm Ti and 150 nm Au, and the lift-off process to fabricate the metasurfaces onto the GeSn membranes. The Ti is used as an adhesion layer, and Au is used because of its chemical stability and low optical losses.

SUPPLEMENTARY MATERIAL

See the supplementary material for additional details on the experimental methodology and modeling framework. This includes extended descriptions of the optical and electrical properties of GeSn devices, the optical setups, the analysis of the optical parameters, and numerical simulations used to interpret the experimental data.

ACKNOWLEDGMENTS

The authors acknowledge support from NSERC Canada, Canada Research Chairs, Canada Foundation for Innovation, Mitacs, PRIMA Québec, and Defense Canada (Innovation for Defense Excellence and Security, IDEaS), the European Union's Horizon Europe research and innovation program under Grant Agreement No. 101070700 (MIRAQLS), and the US Air Force Research Office, Grant No. W911NF-22-1-0277.

AUTHOR DECLARATIONS

Conflict of Interest

The authors have no conflicts to disclose.

Author Contributions

Ziqiang Cai: Conceptualization (equal); Data curation (equal); Formal analysis (equal); Investigation (equal); Methodology (equal); Writing – original draft (lead); Writing – review & editing (equal). **Cédric Lemieux-Leduc**: Formal analysis (supporting); Investigation (equal); Methodology (equal); Software (equal). **Mahmoud R. M. Atalla**: Formal analysis (supporting); Investigation (supporting); Methodology (supporting). **Lu Luo**: Formal analysis (supporting); Investigation (supporting); Methodology (supporting). **Gérard Daligou**: Formal analysis (supporting); Methodology (supporting). **Simone Assali**: Methodology (supporting). **Oussama Moutanabbir**: Conceptualization (lead); Funding acquisition (lead); Investigation (supporting); Methodology (supporting); Project administration (lead); Resources (lead); Supervision (lead); Writing – review & editing (supporting).

DATA AVAILABILITY

The data that support the findings of this study are available within the article and its supplementary material.

03 November 2026 17:51:32

© Author(s) 2026

REFERENCES

[1]M. I. Saleem, A. K. K. Kyaw, and J. Hur, "Infrared photodetectors: Recent advances and challenges toward innovation for image sensing applications," Adv. Opt. Mater. **12**(33), 2401625 (2024).

[2]O. Moutanabbir, S. Assali, X. Gong, E. O'Reilly, C. A. Broderick, B. Marzban, J. Witzens, W. Du, S. Q. Yu, A. Chelnokov, D. Buca, and D. Nam, "Monolithic infrared silicon photonics: The rise of (Si)GeSn semiconductors," Appl. Phys. Lett. **118**(11), 110502 (2021).

[3]X. Liu, J. Zheng, C. Niu, T. Liu, Q. Huang, M. Li, D. Zhang, Y. Pang, Z. Liu, Y. Zuo, and B. Cheng, "Sn content gradient GeSn with strain controlled for high performance GeSn mid-infrared photodetectors," Photonics Res. **10**(7), 1567–1574 (2022).

[4]M. R. M. Atalla, S. Assali, S. Koelling, A. Attiaoui, and O. Moutanabbir, "High-bandwidth extended-SWIR GeSn photodetectors on silicon achieving ultrafast broadband spectroscopic response," ACS Photonics **9**(4), 1425–1433 (2022).

[5]H. Kumar and A. K. Pandey, "GeSn-Based multiple-quantum-well photodetectors for mid-infrared sensing applications," IEEE Trans. Nanobiosci. **21**(2), 175–183 (2022).

[6]C. H. Tsai, K. C. Lin, C. Y. Cheng, K. C. Lee, H. H. Cheng, and G. E. Chang, "GeSn lateral waveguide photodetectors for mid-infrared integrated photonics," Opt. Lett. **46**(4), 864–867 (2021).

[7]L. Luo, M. R. M. Atalla, S. Assali, S. Koelling, and O. Moutanabbir, "Mid-infrared top-gated $Ge_{0.82}Sn_{0.18}$ nanowire phototransistors," Adv. Opt. Mater. **12**(18), 2400096 (2024).

[8]L. Luo, M. R. M. Atalla, S. Assali, S. Koelling, G. Daligou, and O. Moutanabbir, "Mid-infrared imaging using strain-relaxed $Ge_{1-x}Sn_x$ alloys grown on 20 nm Ge nanowires," Nano Lett. **24**(16), 4979–4986 (2024).

[9]M. R. M. Atalla, Y. Kim, S. Assali, D. Burt, D. Nam, and O. Moutanabbir, "Extended-SWIR GeSn LEDs with reduced footprint and efficient operation power," ACS Photonics **10**(5), 1649–1653 (2023).

[10]M. R. M. Atalla, S. Assali, G. Daligou, A. Attiaoui, S. Koelling, P. Daoust, and O. Moutanabbir, "Continuous-wave GeSn light-emitting diodes on silicon with 2.5 μm room-temperature emission," ACS Photonics **11**(3), 1335–1341 (2024).

[11]Y. Kim, S. Assali, D. Burt, Y. Jung, H. J. Joo, M. Chen, Z. Ikonic, O. Moutanabbir, and D. Nam, "Enhanced GeSn Microdisk lasers directly released on Si," Adv. Opt. Mater. **10**(2), 2101213 (2022).

[12]Y. Kim, S. Assali, H. J. Joo, S. Koelling, M. Chen, L. Luo, X. Shi, D. Burt, Z. Ikonic, D. Nam, and O. Moutanabbir, "Short-wave infrared cavity resonances in a single GeSn nanowire," Nat. Commun. **14**(1), 4393 (2023).

[13]Y.-D. Hsieh, J.-H. Lin, R. Soref, G. Sun, H.-H. Cheng, and G.-E. Chang, "Electro-absorption modulation in GeSn alloys for wide-spectrum mid-infrared applications," Commun. Mater. **2**(1), 40 (2021).

[14]M. R. M. Atalla, S. Assali, A. Attiaoui, C. Lemieux-Leduc, A. Kumar, S. Abdi, and O. Moutanabbir, "All-group IV transferable membrane mid-infrared photodetectors," Adv. Funct. Mater. **31**(3), 2006329 (2021).

[15]S. Assali, J. Nicolas, and O. Moutanabbir, "Enhanced Sn incorporation in GeSn epitaxial semiconductors via strain relaxation," J. Appl. Phys. **125**(2), 025304 (2019).

[16]A. Elbaz, D. Buca, N. von den Driesch, K. Pantzas, G. Patriarche, N. Zerounian, E. Herth, X. Checoury, S. Sauvage, I. Sagnes, A. Foti, R. Ossikovski, J. M. Hartmann, F. Boeuf, Z. Ikonic, P. Boucaud, D. Grützmacher, and M. El Kurdi, "Ultra-low-threshold continuous-wave and pulsed lasing in tensile-strained GeSn alloys," Nat. Photonics **14**(6), 375–382 (2020).

[17]Q. Chen, S. Wu, L. Zhang, H. Zhou, W. Fan, and C. S. Tan, "Transferable single-layer GeSn nanomembrane resonant-cavity-enhanced photodetectors for 2 μm band optical communication and multi-spectral short-wave infrared sensing," Nanoscale **14**(19), 7341–7349 (2022).

[18]S. An, S. Wu, C. S. Tan, G. E. Chang, X. Gong, and M. Kim, "Modulation of light absorption in flexible GeSn metal-semiconductor-metal photodetectors by mechanical bending," J. Mater. Chem. C **8**(39), 13557–13562 (2020).

[19]Y. Khan, A. Thielens, S. Muin, J. Ting, C. Baumbauer, and A. C. Arias, "A new frontier of printed electronics: Flexible hybrid electronics," Adv. Mater. **32**(15), 1905279 (2020).

[20]C. Lemieux-Leduc, M. R. M. Atalla, S. Assali, S. Koelling, P. Daoust, L. Luo, G. Daligou, J. Brodeur, S. Kéna-Cohen, Y. A. Peter, and O. Moutanabbir, "Transfer-printed multiple GeSn membrane mid-infrared photodetectors," IEEE J. Sel. Top. Quantum Electron. **31**, 3800410 (2025).

[21]C. Lemieux-Leduc, M. R. M. Atalla, S. Assali, N. Rotaru, J. Brodeur, S. Kéna-Cohen, O. Moutanabbir, and Y.-A. Peter, "Waveguide-coupled mid-infrared GeSn membrane photodetectors on silicon-on-insulator," ACS Photonics **12**, 6343 (2025).

[22]D. S. Grierson, F. S. Flack, M. G. Lagally, and K. T. Turner, "Rolling-based direct-transfer printing: A process for large-area transfer of micro- and nanostructures onto flexible substrates," J. Appl. Phys. **120**(9), 093103 (2016).

[23]Z. Xia, H. Song, M. Kim, M. Zhou, T. H. Chang, D. Liu, X. Yin, K. Xiong, H. Mi, X. Wang, F. Xia, Z. Yu, Z. J. Ma, and Q. Gan, "Single-crystalline germanium nanomembrane photodetectors on foreign nanocavities," Sci. Adv. **3**(7), e1602783 (2017).

[24]N. Yu and F. Capasso, "Flat optics with designer metasurfaces," Nat. Mater. **13**(2), 139–150 (2014).

[25]X. Zhao, T. Lou, Y. Peng, F. Sun, and X. Wei, "Metasurface-based photodetectors: Pursuing superior performance and multifunctionality," ACS Photonics **12**(8), 4096–4118 (2025).

[26]Z. Cai and Y. Liu, "Near-infrared reflection modulation through electrical tuning of hybrid graphene metasurfaces," Adv. Opt. Mater. **10**(6), 2102135 (2022).

[27]Z. Cai, X. Zhang, T. S. Karnik, Y. Xu, T. Kim, J. Hu, and Y. Liu, "Electrically tuning quasi-bound states in the continuum with hybrid graphene-silicon metasurfaces," Adv. Opt. Mater. **13**(8), 2402344 (2025).

[28]H. Jiang, J. Wei, F. Sun, C. Nie, J. Fu, H. Shi, J. Sun, X. Wei, and C. W. Qiu, "Enhanced photogating effect in graphene photodetectors via potential fluctuation engineering," ACS Nano **16**(3), 4458–4466 (2022).

[29]N. Đorđević, R. Schwanninger, M. Yarema, S. Koepfli, O. Yarema, Y. Salamin, N. Lassaline, B. Cheng, N. Yazdani, A. Dorodnyy, Y. M. Fedoryshyn, V. Wood, and J. Leuthold, "Metasurface colloidal quantum dot photodetectors," ACS Photonics **9**(2), 482–492 (2022).

[30]H. Tang, C. J. Chen, Z. Huang, J. Bright, G. Meng, R. S. Liu, and N. Wu, "Plasmonic hot electrons for sensing, photodetection, and solar energy applications: A perspective," J. Chem. Phys. **152**(22), 220901 (2020).

[31]N. C. Wilson, E. Shin, R. E. Bangle, S. B. Nikodemski, J. H. Vella, and M. H. Mikkelsen, "Ultrathin pyroelectric photodetector with integrated polarization-sensing metasurface," Nano Lett. **23**(18), 8547–8552 (2023).

[32]N. T. Yardimci and M. Jarrahi, "Nanostructure-enhanced photoconductive terahertz emission and detection," Small **14**(44), 1802437 (2018).

[33]D. Chen, S. D. March, A. H. Jones, Y. Shen, A. A. Dadey, K. Sun, J. A. McArthur, A. M. Skipper, X. Xue, B. Guo, J. Bai, S. R. Bank, and J. C. Campbell, "Photon-trapping-enhanced avalanche photodiodes for mid-infrared applications," Nat. Photonics **17**(7), 594–600 (2023).

[34]L. Wang, Y. Zhang, B. Wang, Y. Wei, B. Zhang, L. Meng, T. Liu, B. Wang, B. Han, Z. Jiang, and H. Hu, "High-performance infrared Ge-based plasmonic photodetector enhanced by dual absorption mechanism," APL Photonics **5**(9), 096104 (2020).

[35]Z.-X. Zhou, M.-J. Ye, M.-W. Yu, J.-H. Yang, K.-L. Su, C.-C. Yang, C.-Y. Lin, V. E. Babicheva, I. V. Timofeev, and K.-P. Chen, "Germanium metasurfaces with lattice Kerker effect in near-infrared photodetectors," ACS Nano **16**(4), 5994–6001 (2022).

[36]A. Attiaoui, É. Bouthillier, G. Daligou, A. Kumar, S. Assali, and O. Moutanabbir, "Extended short-wave infrared absorption in Group-IV nanowire arrays," Phys. Rev. Appl. **15**(1), 014034 (2021).

[37]Q. Chen, H. Zhou, S. Xu, Y. C. Huang, S. Wu, K. H. Lee, X. Gong, and C. S. Tan, "A route toward high-detectivity and low-cost short-wave infrared photodetection: GeSn/Ge multiple-quantum-well photodetectors with a dielectric nanohole array metasurface," ACS Nano **17**(13), 12151–12159 (2023).

[38]A. Attiaoui, G. Daligou, S. Assali, O. Skibitzki, T. Schroeder, and O. Moutanabbir, "Polarization-tuned fano resonances in all-dielectric short-wave infrared metasurface," Adv. Mater. **35**(28), 2300595 (2023).

[39]J. L. Cui, R. Fang, X. Q. Liu, Y. Y. Wu, Q. X. Huang, Z. P. Liu, F. Yi, Z. Liu, Y. H. Zuo, B. W. Cheng, and J. Zheng, "Comprehensive investigation of GeSn metasurface photodetector for short-wave infrared application," ACS Photonics **11**(10), 4126–4133 (2024).

03 November 2026 17:51:32

© Author(s) 2026

[40]M. Dai, C. Wang, B. Qiang, F. Wang, M. Ye, S. Han, Y. Luo, and Q. J. Wang, "On-chip mid-infrared photothermoelectric detectors for full-stokes detection," Nat. Commun. **13**(1), 4560 (2022).
[41]H. Jiang, Y. Chen, W. Guo, Y. Zhang, R. Zhou, M. Gu, F. Zhong, Z. Ni, J. Lu, C. W. Qiu, and W. Gao, "Metasurface-enabled broadband multidimensional photodetectors," Nat. Commun. **15**(1), 8347 (2024).
[42]X. Liu, Y. Chen, X. Kong, W. Liu, Z. Ni, J. Lu, Q. J. Wang, C. Lee, J. Wei, and C.-W. Qiu, "Metaphotonic photodetectors for direct stokes quantification," Nat. Electron. **8**, 1099 (2025).
[43]C. He, H. He, J. Chang, B. Chen, H. Ma, and M. J. Booth, "Polarisation optics for biomedical and clinical applications: A review," Light: Sci. Appl. **10**(1), 194 (2021).
[44]M. Li, J. Zheng, X. Liu, C. Niu, Y. Zhu, Y. Pang, Z. Liu, Y. Yang, Y. Zuo, and B. Cheng, "GeSn resonance cavity enhanced photodetector with gold bottom reflector for the L band optical communication," Opt. Lett. **47**(17), 4315–4318 (2022).
[45]Z. F. Sadrieva, I. S. Sinev, K. L. Koshelev, A. Samusev, I. V. Iorsh, O. Takayama, R. Malureanu, A. A. Bogdanov, and A. V. Lavrinenko, "Transition from optical bound states in the continuum to leaky resonances: Role of substrate and roughness," ACS Photonics **4**(4), 723–727 (2017).
[46]Y. Yao, R. Shankar, M. A. Kats, Y. Song, J. Kong, M. Loncar, and F. Capasso, "Electrically tunable metasurface perfect absorbers for ultrathin mid-infrared optical modulators," Nano Lett. **14**(11), 6526–6532 (2014).

03 November 2026 17:51:32

© Author(s) 2026